

Evaluation of optical and synthetic aperture radar image fusion methods: a case study applied to Sentinel imagery

Jose Manuel Monsalve-Tellez^{1,2}, Yeison Alberto Garcés-Gómez¹, Jorge Luis Torres-León²

¹Facultad de Ingeniería y Arquitectura, Universidad Católica de Manizales, Manizales, Colombia

²Geomatics Section, Agronomy Research Program, Colombian Oil Palm Research Center-Cenipalma, Bogotá, Colombia

Article Info

Article history:

Received May 6, 2022

Revised Sep 27, 2022

Accepted Oct 1, 2022

Keywords:

Cloud computing

Image fusion methods

Land cover

Optical

Sentinel

Synthetic aperture radar

ABSTRACT

This paper evaluates different optical and synthetic aperture radar (SAR) image fusion methods applied to open-access Sentinel images with global coverage. The objective of this research was to evaluate the potential of image fusion methods to get a greater visual difference in land cover, especially in oil palm crops with natural forest areas that are difficult to differentiate visually. The application of the image fusion methods: Brovey (BR), high-frequency modulation (HFM), Gram-Schmidt (GS), and principal components (PC) was evaluated on Sentinel-2 optical and Sentinel-1 SAR images using a cloud computing environment. The results show that the application of the implemented optical/SAR image fusion methods allows the creation of a synthetic image with the characteristics of both data sources. The multispectral information provided by the optical image and information associated with the geometry and texture/roughness of the land covers, provided by the SAR image, allows a greater differentiation in the visualization of the various land covers, achieving a better understanding of the study area. The fusion methods that visually presented greater characteristics associated with the SAR image were the BR and GS methods. The HFM method reached the best statistical indicators; however, this method did not present significant visual changes in the SAR contribution.

This is an open access article under the [CC BY-SA](https://creativecommons.org/licenses/by-sa/4.0/) license.



Corresponding Author:

Jose Manuel Monsalve-Tellez

Geomatics Section, Agronomy Research Program, Colombian Oil Palm Research Center-Cenipalma

Calle 98#70-91, Bogotá D.C., 11121, Colombia

Email: jmonsalve@cenipalma.org, jose.tellez@ucm.edu.co

1. INTRODUCTION

The significant advances presented in the field of remote sensing related to the development of various sensors onboard satellites for earth observation increasingly enable studies that integrate the combined use of multiple sensors to acquire more information from a particular area of interest [1]–[3]. These developments have made it possible to carry out various investigations related to the determination of land cover, analyze the dynamics of change in different land uses [4], and monitor the growth of deforestation patterns associated with the expansion of agro-industrial production zones using optical and radar satellite platforms [5], [6]. The oil palm agroindustry has shown enormous growth in recent years due to the great demand that the sector has today [7], causing negative impacts on different natural ecosystems [8], especially in the ecosystems of the largest oil palm producing countries in the world such as Indonesia and Malaysia [6]. In Colombia, the oil palm crop is represented by the “*Federación Nacional de Cultivadores de Palma de aceite-Fedepalma*” and is positioned as the largest exporter of palm oil in the Americas and the fourth largest worldwide [9], [10]. Despite the efforts to promote sustainable development of the sector, ecosystems still have impacts, especially in the savanna region [11]. Official land cover maps in Colombia

usually show confusion between the land cover associated with natural forests and oil palm plantations, making it difficult to monitor deforestation caused by this agroindustry. Therefore, the application of remote sensing for monitoring this productive sector has enormous potential, allowing the analysis of large land areas [12].

Currently, it is possible to acquire information from various open-access satellite platforms dedicated to earth observation, which have significantly increased their spatial and temporal resolutions, such as the Sentinel satellites of the Copernicus program of the European Space Agency (ESA). This space program provides information on the earth's surface through a satellite monitoring system with global coverage and revisits periods every six days, using its two operating satellites. This constellation includes satellites with optical sensors, such as Sentinel-2 [13], which capture data associated with the portion of radiation reflected from the earth's surface, and satellites with synthetic aperture radar (SAR) sensors such as Sentinel-1 [14], which captures data concerning the geometry, texture/roughness and water content of land cover on the earth's surface through the intensity of the backscattering signal to the radar sensor [15]. Combining optical and SAR data sources provides more information associated with the land covers in the study area [1], [16].

Some authors have demonstrated the ability to link data from both optical and SAR data sources to increase the quality of land cover determination by implementing synergistic methods [17], [18]. In these investigations, better results were achieved in classifiers when using both sources of information than when using them independently, evaluating diverse levels of land cover classification [19] and applying them in monitoring the growth of oil palm plantations [7], [20]. Optical and SAR image fusion methods have demonstrated the capacity of generating synthetic images with the characteristics of both sources for identifying flooded areas [21] and improving the visual difference of water bodies from other land covers [22]. Thus, it is essential to develop methods that facilitate the integration of various sources of satellite information that are complementary, such as optical and SAR images.

The large volumes of spatial information provided by these global monitoring systems represent an enormous potential for application in the solution of problems such as the continuous monitoring of land cover dynamics over large areas and through cloud computing platforms such as Google Earth Engine (GEE), it is possible to analyze them [18], [21]. Based on this, research has been developed through this platform, where the great benefits it offers in developing projects that link information from different satellite platforms have been exposed [20]. They have been implemented in determining the land cover of large extensions of land [21] and focused on determining areas associated with oil palm growing [23]. In addition, research has been carried out to discriminate the coverages related to this same crop from other types of coverage such as forests and secondary vegetation using SAR images [24], where the potential of using these sources for this purpose is demonstrated, such as the studies carried out by [7], [25], [26].

The objective of this research was to evaluate different image fusion methods applied to Sentinel optical and SAR images that allow increasing the visual identification of different land covers, especially to differentiate between oil palm plantations and natural forest covers. This research will provide a better understanding of the study area and thus visually monitor the dynamics associated with this agribusiness.

2. RESEARCH METHOD

The project was conducted at the *Palmar de la Vizcaína* experimental station (CEPV), of the Oil Palm Research Center-Cenipalma, located on the WGS84 geographic coordinates of 6°59'13" N, 73°40'62" O, in the municipality of Barrancabermeja, Santander, Colombia as shown in Figure 1. Oil palm cultivation in Colombia is distributed in four palm zones, where the central palm zone has the second-largest representation corresponding to 32% of the total area planted in the country [27]. Climatic and topographic conditions are tropical, with mean annual temperatures of 27 °C and mean annual rainfall of 1,600 mm. January is the driest month, and October is the month with the highest precipitation, with relative humidity above 80%. The topographic conditions are characterized by being a mostly flat area with slopes of less than 10%. This area has climatic conditions that favor the establishment of oil palm cultivation. Within the study area, there are areas of natural forests characteristic of tropical regions described above, oil palm plantations, grasslands dedicated mainly to livestock, bare soils, secondary vegetation, and some water bodies.

The images used for the project were selected from the ESA Copernicus program using the GEE cloud computing platform. The cloud-free optical image from the Sentinel-2 satellites [13] acquired on 01/24/2019 with processing level 2A in descending orbit was used. For the generation of the SAR image with a low speckle effect, images from the Sentinel-1 satellite acquired from 11/24/2018 to 03/24/2019 with ground range detected (GRD) processing level in descending orbit was selected. This range of dates corresponds to a dry season with a monthly rainfall of fewer than 90 millimeters, so the SAR images chosen in this study present similar humidity conditions. In this case, eight SAR images acquired during the period mentioned above were used.

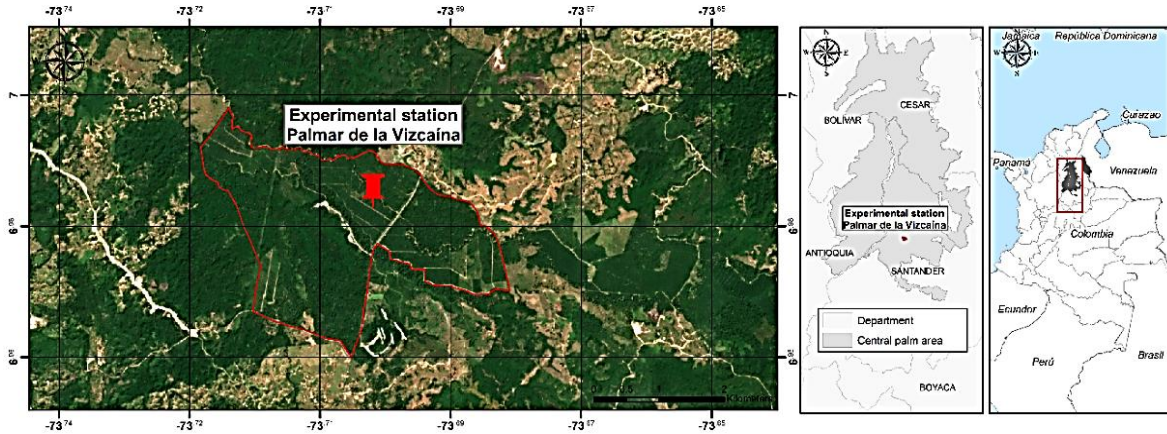


Figure 1. Location of the study area, central palm zone, Santander, Colombia

The methodology implemented is presented in Figure 2. As a first step, the SAR image must be preprocessed to reduce the speckle effect of “salt and pepper” caused by the interaction of the radar signal waves on the different textures and structural conformation of the land cover [28], [29]. For this process, we applied the multitemporal speckle reduction methodology proposed by Quegan and Yu [30] and implemented it in GEE by Mullissa *et al.* [31], which consists of edge noise reduction where low-intensity noise and invalid data present in the scene are removed. Speckle filtering is performed by averaging the backscattering decibel values current in several images with acquisition dates as close as possible, in this study case we use the images acquired in the period mentioned above. The normalization process of the backscatter decibel values of the SAR image is performed between 0 and 1 to be comparable with the values present in the optical image [32].

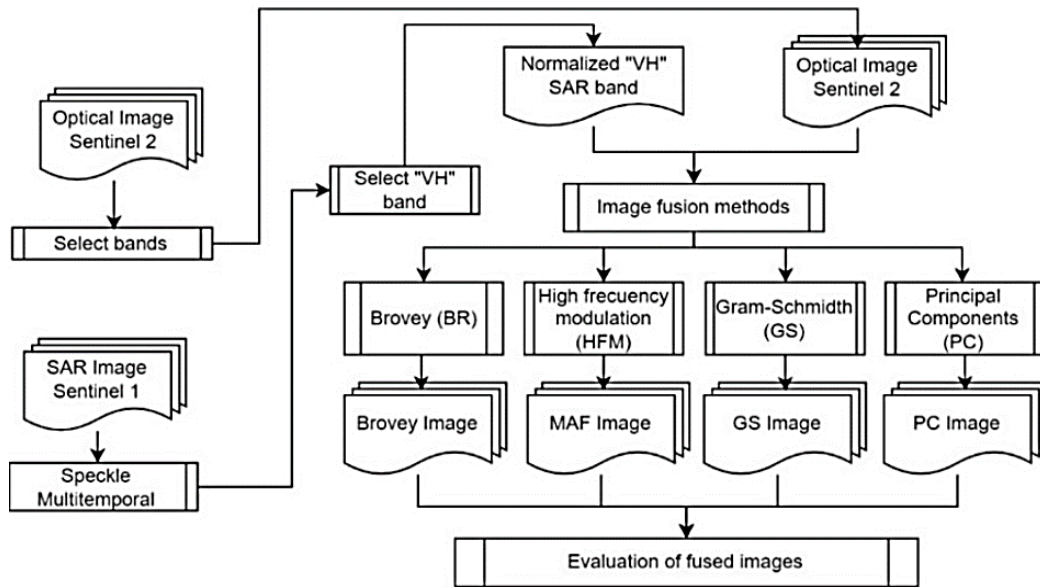


Figure 2. The overall workflow used in this study is described in the pre-processing, image fusion process, and evaluation of image fusion methods

The bands selected for the optical image are associated with the visual and near-infrared spectrum from B2 to B8A, B9, and shortwave infrared B11 and B12. For the SAR case, the vertical emission and horizontal reception (VH) polarization bands were selected from the SAR image. This band was set based on the principle of wave interaction with surface objects [7]. Given the wavelength at which Sentinel-1 operates (C-band of 5.55 cm) [14], the VH polarization presents a lower reflection when interacting with oil palm

leaves than with the leaves of trees in forests, which allows better differentiation between this coverage and those associated with natural forests [33].

The image fusion methods evaluated in this research are Brovey (BR) method [34], the high-frequency modulation (HFM) method [35], the Gram-Schmidt (GS) method [36], and the principal components (PC) method [37]. For the statistical evaluation of optical/SAR image fusion results, widely studied indexes are found in the literature [38], [39]. In this case, five statistical indicators are implemented to evaluate the quality of the results: root mean square error (RMSE), standard deviation (SDT), peak signal-to-noise ratio (PSNR), correlation coefficient (CC), and relative dimensionless global error in synthesis (ERGAS) [40]. In (1) to (5), MS represents the original multispectral image, F represents the fused image, and M and N are the total numbers of rows and columns, respectively.

Root mean square error (RMSE) (1) allows measurement of the error associated with two sets of data; in this case, the results acquired from the fused image compared to the original image. SDT (2) estimates the image's contrast, where the higher the deviation value, the greater the richness of the information available. The value of the dispersion of the data is calculated around its arithmetic to mean. PSNR (3) measures the noise present in the fused image compared to the original image, where the higher the value of this index, the lower the noise of the fused image. CC (4) evaluates the correlation between the original image and the fused image, where a higher degree of correlation means a good result of the fusion process between the images. ERGAS (5) measures the overall quality of the image fusion process. Unlike the previous ones, this index performs the calculation considering all the bands of the fused image, resulting in a value that the smaller it is, the better the fusion result.

$$\text{RMSE} = \frac{1}{M*N} \sqrt{\sum_{m=1}^M \sum_{n=1}^N (F - \text{MS})^2} \quad (1)$$

$$\text{SDT} = \sqrt{\frac{1}{M*N} \sum_{m=1}^M \sum_{n=1}^N (F - \bar{F})^2} \quad (2)$$

$$\text{PSNR} = 10 \log \left(\frac{F_{\max}^2}{\frac{1}{M*N} \sum_{m=1}^M \sum_{n=1}^N (F - \bar{F})^2} \right) \quad (3)$$

$$\text{CC} = \frac{\sum_{m=1}^M \sum_{n=1}^N [(F - \bar{F}) * (\text{MS} - \overline{\text{MS}})]}{\sqrt{\sum_{m=1}^M \sum_{n=1}^N (F - \bar{F})^2 * \sum_{m=1}^M \sum_{n=1}^N (\text{MS} - \overline{\text{MS}})^2}} \quad (4)$$

$$\text{ERGAS} = 100 \frac{h}{l} \sqrt{\frac{1}{n} \sum_{i=1}^n \left[\frac{\text{RSME}(i)}{\text{Mean}(i)} \right]^2} \quad (5)$$

where in SDT, PSNR, and CC, \bar{F} represents the average of the fused image values. In PSNR, F_{\max}^2 represents the maximum value in the fused image. In CC, $\overline{\text{MS}}$ represents the multispectral image values. In ERGAS, h and l are the spatial resolutions of the fused and original image respectively, n is the number of bands in the image, $\text{RSME}(i)$ represents the root mean squared error of the i band and $\text{Mean}(i)$ represents the average of the i band.

3. RESULTS AND DISCUSSION

The first step was the preprocessing of the images. In the case of the optical image, since it is at processing level 2A, corresponding to surface reflectivity values, no additional processing was required. In the case of the SAR image, since it is at a GRD processing level, the multitemporal speckle reduction method was applied, and a median filter with a 3×3 moving window was applied. Using the multitemporal speckle reduction method, it was possible to create a SAR image in which the geometric and textural characteristics associated with the different coverages present in the study area can be better appreciated. As well as the results achieved by Quegan and Yu [30], the potential of using consecutive SAR images to reduce noise caused by the speckle effect and thus expand the possibilities of using SAR data in various applications, such as the fusion of data acquired from different satellite sources. The result of the multitemporal speckle reduction is shown in Figure 3, where a single SAR image is presented on the left and the result of the multitemporal speckle reduction method using several consecutive SAR images is shown on the right. This process allows to create a SAR image with truly little speckle noise effect, visualizing better the different coverages in the study area, allowing to achieve better results in the optical and SAR image fusion methods.

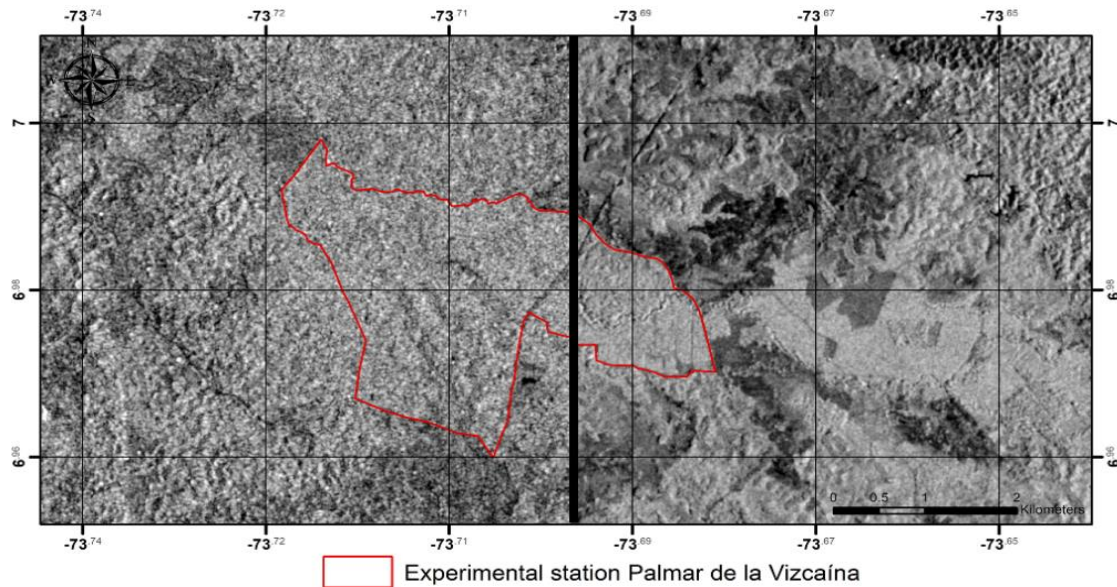


Figure 3. Multitemporal speckle reduction method applied in the “VH” band of Sentinel-1 SAR image

3.1. Optical/SAR image fusion methods

This section shows the results of applying each optical and SAR image fusion method. For each of the fusion methods implemented, a synthetic image of eleven bands with a spatial resolution of 10 m each was created, containing the information from both sources. The result of the BR method shows an enhancement in the texture of the coverages without affecting their geometries. Visually, the quality of the resulting image allows differentiation of the different coverages present in the study area. A noticeable differentiation was found between the coverages associated with water bodies provided by the SAR image due to the specular interaction of the radar wave. Comparable results to that found by [28], [39], which presented a notorious visual difference of water bodies with the other land covers when applying optical/SAR image fusion methods.

In the case of HFM method, the high-pass (HP) and low-pass (LP) filters were first applied to the normalized SAR image, which are the inputs required for the application of this fusion method. Subsequently, the HFM method was calculated, finding a very high similarity with the original image. The enhancements associated with the texture of the coverages are not as noticeable as in the previous method. The results achieved by [29], [41] demonstrate the efficiency of the application of HP and LP filters in image fusion methods for the reduction of noise caused by speckles in the SAR image, which is reflected in the result of this research. It has been shown that using these filters in image fusion methods significantly improves the clarity of the objects in the study area [42]. However, an improvement in the sharpness of the image is evidenced, where differentiation between the several types of coverages and linear objects present in the scene, such as access roads and delimitation of the lots within the experimental station, is due to the contribution of the enhancement of the HP filter in the fusion method.

The image generated by the GS method enhances the characteristics of the SAR image, such as the texture associated with the coverages, and visual differences between them can be appreciated. As a result of the BR method, a very noticeable differentiation is observed between the coverages associated with oil palm cultivation and forest coverages. A notorious enhancement is also observed in linear objects such as access roads, lot boundaries, and clear differentiation between grasslands and bare soil.

Finally, the result of PC the method, as well as the HFM method, presents a very high similarity with the original image. No noticeable modifications are observed in the SAR image contribution regarding the texture associated with the coverages, as it is possible to appreciate in the BR and GS methods. The similarity was found in the results presented by Quan *et al.* [39], which showed a notorious difference in the visualization of colors associated with the different land covers. In contrast, the GS method better preserves the optical image's original colors. In contrast, the PC method presented more significant alterations.

Figure 4 shows the histograms of values per band for each of the fusion methods evaluated. The blue color represents the original values of the Sentinel-2 image, and the orange color represents the values of the corresponding fusion method. In the case of BR method, a shift was evidenced due to the change in the values of the resulting image, in bands B2, B3, B4, B11, and B12, there is a similar trend in the distribution

of the data compared with those of the original bands. However, in the other bands, primarily significant distortions compared to the histograms of the original bands. In all cases, an increase in the range of the data was observed. In the histogram for the HFM method, it was observed that there is a very high relationship between the values of the merged image compared to the distribution of the values of the original bands. This implies that a very high similarity was achieved between the image created from the optical and radar fusion process compared to the original image. In the histogram of GS method, the B2, B3, B4, B5, B11, and B12 bands presented a noticeable change in their distribution compared to the original bands. However, the data range was not altered. For bands B6, B7, B8, B8A, and B9, some changes were observed when compared with the values of the original image bands, but they were not very significant. As shown in the comparison of the histograms for the PC method, B2, B3, B4, B5, B11, and B12 bands presented significant distortions. In contrast, the other bands are highly like the original image. This may be because the one principal component replaced by the SAR image showed a high correlation with bands B6, B7, B8, B8A, and B9.

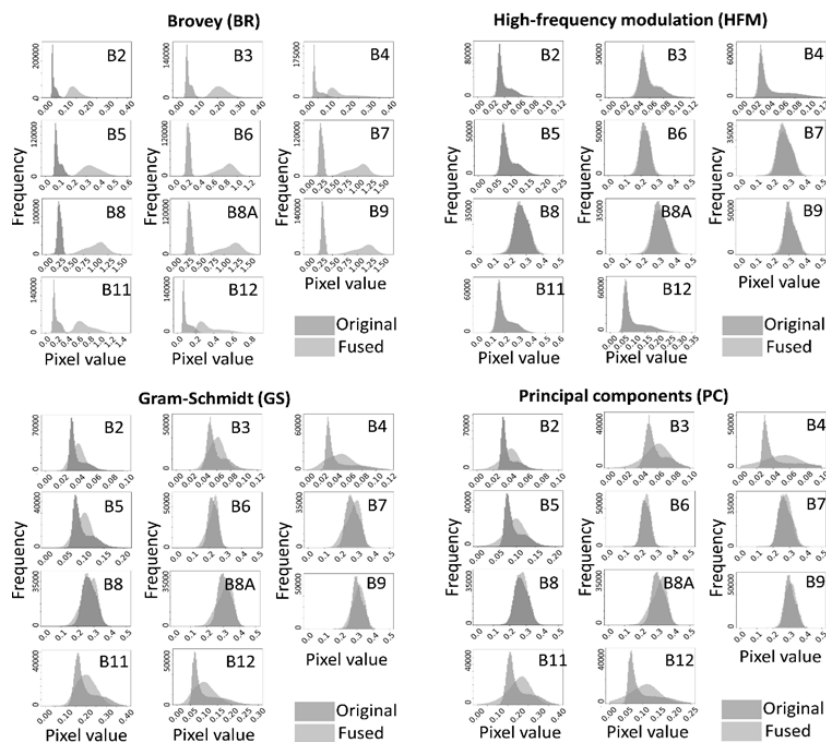


Figure 4. Histogram of values per band for each of the fusion methods evaluated

Figure 5 shows the comparison of the different fusion methods implemented. Notable differences were observed in the results of the image fusion methods between the optical image, which can be seen in Figure 5(a) the SAR image, which can be seen in Figure 5(b), especially in the areas of natural forests and oil palm crops due to differences in the backscatter values presented in the SAR image, improving the visual quality of the definition of linear elements such as access roads and delimitation of lots within the experimental station. This was evidenced in the BR method, which can be seen in Figure 5(c) which presented good differentiation in both land covers and linear elements. The method that best discriminated linear objects corresponds to the HFM method can be seen in Figure 5(d) due to the improvement provided by the HP filter. In the GS method can be seen Figure 5(e) large differences were found between forest and oil palm land cover, like that observed by the BR method. The CP method, can be seen in Figure 5(f), presented the largest visual distortions of the image where cover differentiation was not as noticeable.

As demonstrated by Li *et al.* [43], the generation of a synthetic image containing the characteristics of both optical and SAR information sources allows better visualization of the land cover associated with water bodies and flat surfaces because of the specular interaction of the radar signal. In addition, as stated by Sarzynski *et al.* [20], the linking of information captured by optical and SAR sensors offers a significant advantage in the differentiation of coverages associated with areas of oil palm crops and forests, verifying the results achieved in this study by the BR and GS fusion methods, where more significant differences between these two coverages are observed.

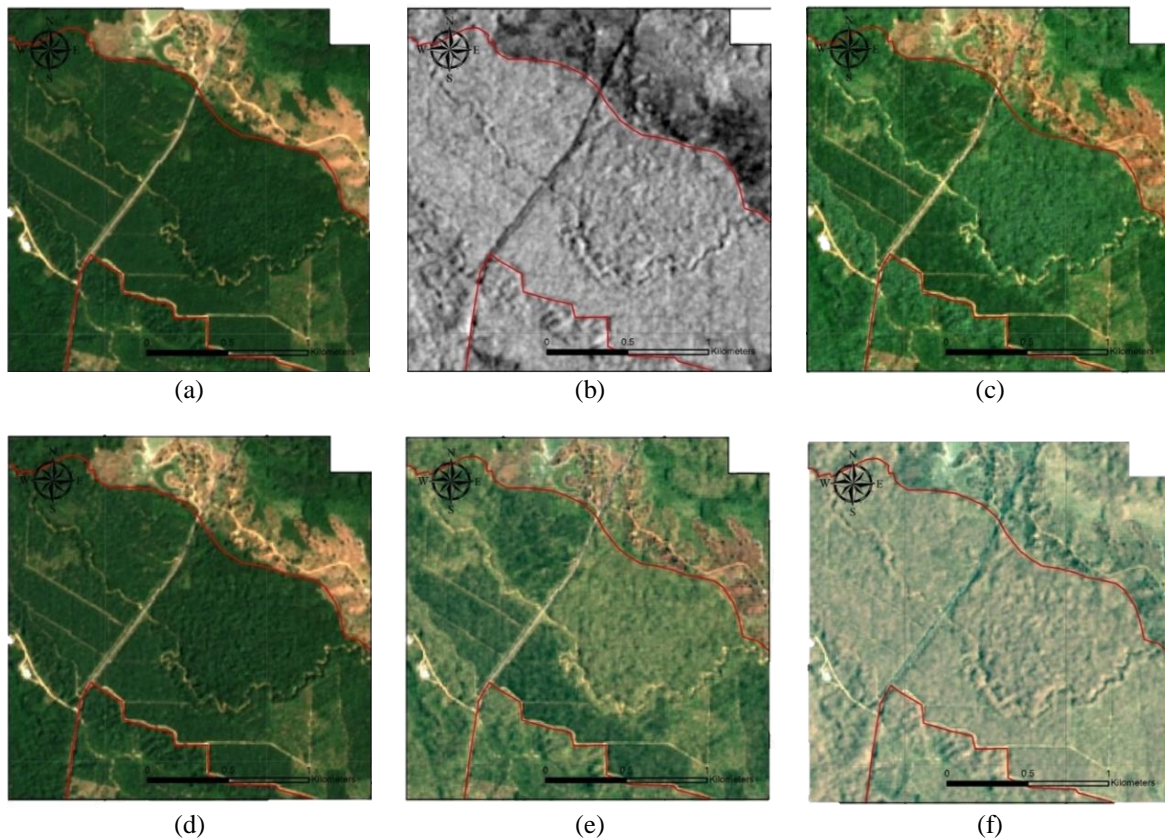


Figure 5. Comparison of images evaluated (a) optical image in true color (RGB) combination, (b) SAR image in VH polarization, and (c) BR, (d) HFM, (e) GS, and (f) CP methods in true color (RGB) combination

3.2. Evaluation of optical/SAR image fusion methods

This section presents the results achieved with the statistical indicators: RMSE, SDT, PSNR, CC, and ERGAS to evaluate the quality of the fusion methods. For all fusion methods, the RMSE values were remarkably close to zero, indicating that the associated error in comparing the fused and original images is very low. This is also the case with the SDT, which for all methods was close to zero, with a differential increase in the case of BR method, especially between bands B7, B8, B9A, and B9. Regarding the evaluation of the PSNR index, it was observed that the values for all the evaluated methods were high, which means that a very high noise level was not found in the images compared to the original image. The method that evidenced a higher amount of noise using the PSNR index was the BR method. The method that achieved the highest CC was the HFM method, reaching values higher than 0.9 in all bands, except in bands B8A and B9, which presented a value of 0.89 and 0.83, respectively. For the BR and PC methods, very high CC values were reached in bands B2, B3, B4, B5, B11, and B12. However, the other bands achieved shallow correlation values, which coincide with an increase in the error of the RMSE and PSNR indexes. These results are like those presented by Quan *et al.* [39], where the average CC of the fused image bands by the GS method presented higher values than the PC method in different study areas evaluated. In addition, he also observed better results in both SDT and PSNR. The HFM method reached the best ERGAS index, followed by the GS and PC methods, meaning that the fusion processes with SAR images did not present significant distortions. In the case of the BR method, mean values were obtained in the result of ERGAS index. Table 1 shows the results of the statistical indicators for the BR and HFM methods and Table 2 the results for the GS and PC methods.

In the literature, it is possible to find some authors who point out the importance of implementing statistical metrics to measure the quality of the results reached with fusion methods. In the results presented by Kulkarni and Rege [38] a similarity was found between the CC values in the optical spectrum bands B3 and B4, with a significant decrease in the near-infrared spectrum bands B8 and B8A (<0.3). However, they differ in the results for the shortwave infrared bands B11 and B12, where in this study, a high CC was achieved (>0.9) in the HFM and BR methods. A similar result was also found in the ERGAS index, where the PC method presented a better result than the BR method.

Table 1. Result of the quality evaluation of the BR and HFM methods

Sentinel-2 bands	Brovey (BR)				High-frequency modulation (HFM)			
	RMSE	SDT	PSNR	CC	RMSE	SDT	PSNR	CC
Band2	0.00013	0.03075	21.196	0.760	0.00000	0.01273	42.712	0.961
Band3	0.00019	0.04058	19.050	0.711	0.00001	0.01726	40.470	0.955
Band4	0.00015	0.07272	20.647	0.921	0.00001	0.02781	41.206	0.984
Band5	0.00030	0.06888	14.716	0.744	0.00001	0.02875	36.971	0.959
Band6	0.00073	0.14446	7.664	0.489	0.00002	0.03574	32.157	0.880
Band7	0.00090	0.20041	7.575	0.630	0.00002	0.04794	32.065	0.903
Band8	0.00089	0.20593	7.980	0.661	0.00002	0.05038	32.363	0.916
Band8A	0.00101	0.21603	7.424	0.586	0.00003	0.05033	32.143	0.889
Band9	0.00100	0.20225	9.337	0.493	0.00003	0.04219	32.260	0.833
Band11	0.00063	0.16429	9.095	0.802	0.00002	0.06406	35.099	0.966
Band12	0.00033	0.13907	13.980	0.914	0.00001	0.05067	36.656	0.983
ERGAS		0.3200				0.0098		

Table 2. Result of the quality evaluation of the GS and PC methods

Sentinel-2 bands	Gram-Schmidt (GS)				Principal component (PC)			
	RMSE	SDT	PSNR	CC	RMSE	SDT	PSNR	CC
Band2	0.00001	0.00971	31.727	0.664	0.00002	0.01248	28.311	0.144
Band3	0.00002	0.01295	28.561	0.546	0.00002	0.01704	27.492	0.283
Band4	0.00002	0.02140	25.576	0.681	0.00005	0.02781	22.845	0.014
Band5	0.00003	0.02140	24.145	0.522	0.00004	0.02895	23.548	0.171
Band6	0.00003	0.03386	25.429	0.640	0.00003	0.02688	26.098	0.612
Band7	0.00003	0.04684	26.152	0.790	0.00006	0.03765	22.340	0.265
Band8	0.00004	0.04973	25.843	0.780	0.00005	0.03835	22.377	0.378
Band8A	0.00004	0.04859	26.163	0.770	0.00005	0.03737	22.472	0.317
Band9	0.00002	0.03742	28.238	0.853	0.00005	0.03392	22.685	0.361
Band11	0.00006	0.04934	23.388	0.589	0.00010	0.06641	17.418	0.072
Band12	0.00004	0.03961	23.244	0.684	0.00009	0.05256	17.691	-0.081
ERGAS		0.0275				0.0488		

4. CONCLUSION

The implemented multitemporal reduction of speckle noise demonstrated its enormous usefulness in increasing the quality of SAR images, facilitating their interpretation, and expanding the great applications submitted by SAR systems in various fields. The results presented by this method made it possible to generate fused images of very high quality and without significant affectations caused by the speckle effect of the SAR images. In this research, it was demonstrated that the information from Sentinel-2 optical sensors and Sentinel-1 SAR are complementary and by applying image fusion methods it is possible to generate a new synthetic image with both characteristics. In this way, it is possible to better understand the characteristics present in a study area by enhancing the coverage's geometric and texture/roughness characteristics without losing the visualization of the color composition provided by the optical image. The methods that visually presented the most characteristic features of the SAR image are the BR and GS methods. Despite reaching the best statistical indicators, the HFM and PC methods did not show significant visual changes regarding SAR image contribution. The high capacity of cloud computing platforms and the high availability of information on issues related to earth observation data, such as GEE, demonstrates the potential of using image fusion techniques in any area of the world where detailed analysis of the behavior of the different coverages present in the study area is required. For future research, it is recommended to implement optical and SAR image fusion methods applied to Sentinel imagery to assess land cover classification accuracy. Since the fusion methods evaluated allow the creation of a synthetic image with all the bands of the original image, in this case, eleven bands, are useful for classification algorithms.

ACKNOWLEDGEMENTS

Acknowledgments to the "Universidad Católica de Manizales" and the master's program in remote sensing for the support and guidance provided in the project's development. Thanks to the "Centro de Investigación en Palma de Aceite-CENIPALMA", for the technical support and financing of this research. Finally, thanks to the European Space Agency (ESA) for providing free optical and SAR data.

REFERENCES




- [1] N. Joshi *et al.*, "A review of the application of optical and radar remote sensing data fusion to land use mapping and monitoring," *Remote Sensing*, vol. 8, no. 1, Jan. 2016, doi: 10.3390/rs8010070.
- [2] M. Schmitt, F. Tupin, and X. X. Zhu, "Fusion of SAR and optical remote sensing data-challenges and recent trends," in *2017 Evaluation of optical and synthetic aperture radar image fusion methods ... (Jose Manuel Monsalve-Tellez)*

- IEEE International Geoscience and Remote Sensing Symposium (IGARSS)*, Jul. 2017, pp. 5458–5461, doi: 10.1109/IGARSS.2017.8128239.
- [3] S. Dhingra and D. Kumar, “A review of remotely sensed satellite image classification,” *International Journal of Electrical and Computer Engineering (IJECE)*, vol. 9, no. 3, pp. 1720–1731, Jun. 2019, doi: 10.11591/ijece.v9i3.pp1720-1731.
 - [4] A. Mercier *et al.*, “Evaluation of Sentinel-1 and 2 time series for land cover classification of forest-agriculture mosaics in temperate and tropical landscapes,” *Remote Sensing*, vol. 11, no. 8, Apr. 2019, doi: 10.3390/rs11080979.
 - [5] D. K. Seo, Y. H. Kim, Y. D. Eo, M. H. Lee, and W. Y. Park, “Fusion of SAR and multispectral images using random forest regression for change detection,” *ISPRS International Journal of Geo-Information*, vol. 7, no. 10, Oct. 2018, doi: 10.3390/ijgi7100401.
 - [6] A. Poortinga *et al.*, “Mapping plantations in Myanmar by fusing Landsat-8, Sentinel-2 and Sentinel-1 data along with systematic error quantification,” *Remote Sensing*, vol. 11, no. 7, Apr. 2019, doi: 10.3390/rs11070831.
 - [7] L. Li, J. Dong, S. Njeudeng Tenku, and X. Xiao, “Mapping oil palm plantations in Cameroon using PALSAR 50-m orthorectified mosaic images,” *Remote Sensing*, vol. 7, no. 2, pp. 1206–1224, Jan. 2015, doi: 10.3390/rs70201206.
 - [8] J. De Alban, G. Connette, P. Oswald, and E. Webb, “Combined Landsat and L-Band SAR data improves land cover classification and change detection in dynamic tropical landscapes,” *Remote Sensing*, vol. 10, no. 2, Feb. 2018, doi: 10.3390/rs10020306.
 - [9] J. Mesa Dishington, “Innovation and sustainability in the oil palm agribusiness in Colombia (in Spanish),” *Revista Palmas*, vol. 40, pp. 9–18, 2019.
 - [10] A. M. Galvez Valencia, Y. A. Garcés-Gomez, E. L. Lemus Rodriguez, and M. A. Arango Argoti, “Predictive model of water stress in tenera oil palm by means of spectral signature methods,” *International Journal of Electrical and Computer Engineering (IJECE)*, vol. 11, no. 3, pp. 2680–2687, Jun. 2021, doi: 10.11591/ijece.v11i3.pp2680-2687.
 - [11] L. E. P. Vargas, W. F. Laurance, G. R. Clements, and W. Edwards, “The impacts of oil palm agriculture on Colombia’s biodiversity: what we know and still need to know,” *Tropical Conservation Science*, vol. 8, no. 3, pp. 828–845, Sep. 2015, doi: 10.1177/194008291500800317.
 - [12] N. Torbick, L. Ledoux, W. Salas, and M. Zhao, “Regional mapping of plantation extent using multisensor imagery,” *Remote Sensing*, vol. 8, no. 3, Mar. 2016, doi: 10.3390/rs8030236.
 - [13] ESA, *Sentinel-2 user handbook*. ESA Standard Document, 2015.
 - [14] ESA, *Sentinel-1 user handbook*. ESA User Guide, 2013.
 - [15] L. D. Robertson *et al.*, “C-band synthetic aperture radar (SAR) imagery for the classification of diverse cropping systems,” *International Journal of Remote Sensing*, vol. 41, no. 24, pp. 9628–9649, Dec. 2020, doi: 10.1080/01431161.2020.1805136.
 - [16] R. Sonobe, Y. Yamaya, H. Tani, X. Wang, N. Kobayashi, and K. Mochizuki, “Assessing the suitability of data from Sentinel-1A and 2A for crop classification,” *GIScience and Remote Sensing*, vol. 54, no. 6, pp. 918–938, Nov. 2017, doi: 10.1080/15481603.2017.1351149.
 - [17] R. Fieuzal, C. Marais Sicre, and F. Baup, “Estimation of corn yield using multi-temporal optical and radar satellite data and artificial neural networks,” *International Journal of Applied Earth Observation and Geoinformation*, vol. 57, pp. 14–23, May 2017, doi: 10.1016/j.jag.2016.12.011.
 - [18] N. Verde *et al.*, “National scale land cover classification for ecosystem services mapping and assessment, using multitemporal Copernicus EO data and Google Earth Engine,” *Remote Sensing*, vol. 12, no. 20, Oct. 2020, doi: 10.3390/rs12203303.
 - [19] J. R. Mancera Florez, “Evaluation of Sentinel-1A radar images and Sentinel-2A multispectral images in land cover classification at different levels of detail,” (in Spanish), Universidad Nacional de Colombia-Sede Bogota, 2019.
 - [20] T. Sarzynski, X. Giam, L. Carrasco, and J. S. H. Lee, “Combining radar and optical imagery to map oil palm plantations in Sumatra, Indonesia, using the Google Earth Engine,” *Remote Sensing*, vol. 12, no. 7, Apr. 2020, doi: 10.3390/rs12071220.
 - [21] M. Zhang *et al.*, “Automatic high-resolution land cover production in Madagascar using Sentinel-2 time series, tile-based image classification and Google Earth Engine,” *Remote Sensing*, vol. 12, no. 21, Nov. 2020, doi: 10.3390/rs12213663.
 - [22] Z. Shao, W. Wu, and S. Guo, “IHS-GTF: A fusion method for optical and synthetic aperture radar data,” *Remote Sensing*, vol. 12, no. 17, Aug. 2020, doi: 10.3390/rs12172796.
 - [23] C. Pohl, K. L. Chong, and J. van Genderen, “Multisensor approach to oil palm plantation monitoring using data fusion and GIS,” *Monitoring oil palm plantations for sustainability*, 2015.
 - [24] S. Darmawan *et al.*, “The potential scattering model for oil palm phenology based on spaceborne X-, C-, and L-Band polarimetric SAR imaging,” *Journal of Sensors*, pp. 1–14, Mar. 2021, doi: 10.1155/2021/6625774.
 - [25] Y. W. Kee, A. R. M. Shariff, A. M. Sood, and L. Nordin, “Application of SAR data for oil palm tree discrimination,” *IOP Conference Series: Earth and Environmental Science*, vol. 169, Jul. 2018, doi: 10.1088/1755-1315/169/1/012065.
 - [26] C. Pohl, “Mapping palm oil expansion using SAR to study the impact on the CO₂ cycle,” *IOP Conference Series: Earth and Environmental Science*, vol. 20, Jun. 2014, doi: 10.1088/1755-1315/20/1/012012.
 - [27] Cenipalma, “Portal GeoPalma. Tablero Catastro: Geoservicio Catastro Físico,” *Centro de Investigación en Palma de aceite*. Bogotá, D.C., Colombia, 2021, Accessed: Jan. 09, 2022. [Online]. Available: <https://geopalma.cenipalma.org>
 - [28] Y. Byun, J. Choi, and Y. Han, “An area-based image fusion scheme for the integration of SAR and optical satellite imagery,” *IEEE Journal of Selected Topics in Applied Earth Observations and Remote Sensing*, vol. 6, no. 5, pp. 2212–2220, Oct. 2013, doi: 10.1109/JSTARS.2013.2272773.
 - [29] T. Chu, Y. Tan, Q. Liu, and B. Bai, “Novel fusion method for SAR and optical images based on non-subsampled shearlet transform,” *International Journal of Remote Sensing*, vol. 41, no. 12, pp. 4590–4604, Jun. 2020, doi: 10.1080/01431161.2020.1723175.
 - [30] S. Quegan and J. J. Yu, “Filtering of multichannel SAR images,” *IEEE Transactions on Geoscience and Remote Sensing*, vol. 39, no. 11, pp. 2373–2379, 2001, doi: 10.1109/36.964973.
 - [31] A. Mullissa *et al.*, “Sentinel-1 SAR backscatter analysis ready data preparation in Google Earth Engine,” *Remote Sensing*, vol. 13, no. 10, May 2021, doi: 10.3390/rs13101954.
 - [32] H. Zhang, H. Lin, and Y. Li, “Impacts of feature normalization on optical and SAR data fusion for land use/land cover classification,” *IEEE Geoscience and Remote Sensing Letters*, vol. 12, no. 5, pp. 1061–1065, May 2015, doi: 10.1109/LGRS.2014.2377722.
 - [33] M. Lazbecky, S. Lhota, T. Penaz, and D. Klushina, “Application of Sentinel-1 satellite to identify oil palm plantations in Balikpapan Bay,” *IOP Conference Series: Earth and Environmental Science*, vol. 169, Jul. 2018, doi: 10.1088/1755-1315/169/1/012064.
 - [34] D. Yıldırım and O. Güngör, “A novel image fusion method using IKONOS satellite images,” *Journal of Geodesy and Geoinformation*, vol. 1, no. 1, pp. 27–34, 2012, doi: 10.9733/jgg.170512.1.




- [35] Y. Jia, M. Wu, and X. Zhang, "An improved high frequency modulating fusion method based on modulation transfer function filters," *ISPRS Annals of the Photogrammetry, Remote Sensing and Spatial Information Sciences*, vol. 1–7, pp. 285–290, Jul. 2012, doi: 10.5194/isprannals-1-7-285-2012.
- [36] C. A. Laben and B. V. Brower, "Process for enhancing the spatial resolution of multispectral imagery using pan-sharpening." Google Patents, 2000.
- [37] M. Gonzalez-Audicana, J. L. Saleta, R. G. Catalan, and R. Garcia, "Fusion of multispectral and panchromatic images using improved IHS and PCA mergers based on wavelet decomposition," *IEEE Transactions on Geoscience and Remote Sensing*, vol. 42, no. 6, pp. 1291–1299, Jun. 2004, doi: 10.1109/TGRS.2004.825593.
- [38] S. C. Kulkarni and P. P. Rege, "Pixel level fusion techniques for SAR and optical images: A review," *Information Fusion*, vol. 59, pp. 13–29, Jul. 2020, doi: 10.1016/j.inffus.2020.01.003.
- [39] Y. Qian, Y. Tong, W. Feng, G. Dauphin, W. Huang, and M. Xing, "A novel image fusion method of multi-spectral and SAR images for land cover classification," *Remote Sensing*, vol. 12, no. 22, Nov. 2020, doi: 10.3390/rs12223801.
- [40] Q. Du, N. H. Younan, R. King, and V. P. Shah, "On the performance evaluation of pan-sharpening techniques," *IEEE Geoscience and Remote Sensing Letters*, vol. 4, no. 4, pp. 518–522, Oct. 2007, doi: 10.1109/LGRS.2007.896328.
- [41] A. Sharma and T. Gulati, "Change detection from remotely sensed images based on stationary wavelet transform," *International Journal of Electrical and Computer Engineering (IJECE)*, vol. 7, no. 6, pp. 3395–3401, Dec. 2017, doi: 10.11591/ijece.v7i6.pp3395-3401.
- [42] Q. Li, X. Yang, W. Wu, K. Liu, and G. Jeon, "Multi-focus image fusion method for vision sensor systems via dictionary learning with guided filter," *Sensors*, vol. 18, no. 7, p. 2143, Jul. 2018, doi: 10.3390/s18072143.
- [43] D. Li, Y. Zhang, X. Dong, X. Shi, and W. Zhai, "A HSV-based fusion of InIRA SAR and Google Earth optical images," in *2018 Asia-Pacific Microwave Conference (APMC)*, Nov. 2018, pp. 848–850, doi: 10.23919/APMC.2018.8617352.

BIOGRAPHIES OF AUTHORS






Jose Manuel Monsalve-Tellez    is a topographic engineer from Universidad del Valle and a master in remote sensing from Universidad Católica de Manizales, Colombia. He serves as Geographic Information Systems and Remote Sensing researcher in the Geomatics area, attached to the Agronomy program, of the Oil Palm Research Center, Cenipalma. Her research interests include the application of remote sensing in precision agriculture, image fusion process, and artificial intelligence. He can be contacted at jmonsalve@cenipalma.org.



Yeison Alberto Garcés-Gómez    received a bachelor's degree in Electronic Engineering, and master's and Ph.D. degrees in Engineering from Electrical, Electronic and Computer Engineering Department, Universidad Nacional de Colombia, Manizales, Colombia, in 2009, 2011, and 2015, respectively. He is a full professor at the Academic Unit for Training in Natural Sciences and Mathematics, Universidad Católica de Manizales, and teaches several courses such as Experimental Design, Statistics, and Physics. His main research focus is on applied technologies, embedded systems, power electronics, and power quality, but also many other areas of electronics, signal processing, and didactics. He can be contacted at ygarcés@ucm.edu.co.



Jorge Luis Torres-León    is a system and computer engineer from Universidad Industrial de Santander. Master in Geoinformation Sciences and Earth Observation, with emphasis in Geoinformatics from the University of Twente (Netherlands, ITC). In previous years he served as GeoInformation and Technology Manager for the General Directorate of Military Geographic Studies of the Ministry of Defense of Saudi Arabia. Today he serves as Leader of the Geomatics area, a position he has held for the last 9 years. At this moment he directs the lines of research in geographic information systems, remote sensing, and precision agriculture, attached to the Agronomy program of the Research Directorate of Cenipalma. Member of the International Society of Precision Agriculture (ISPA) and certified drone pilot in Colombia. He can be contacted at jltorres@cenipalma.org.